Indian Journal of Chemistry
Vol. 61, January 2022, pp. 37-42

A 3D Co(II) compound: Crystal structure and protective activity on chronic nephritis

Xiu-Zhen Shi[a], Ai-Li Guo[a], Kai Fu[a], Yan He[a], Qin Li[b] & Qiong Luo[b,*]

[a]Department of Nephrology, General Hospital of the Yangtze River Shipping, Wuhan, Hubei, China

[b]Department of Endocrinology, General Hospital of the Yangtze River Shipping, Wuhan, Hubei, China

*E-mail: drluoqiong@163.com

Received 17 September 2021; revised and accepted 28 December 2021

In the current study, via applying a mixed-ligand strategy, a Co(II) coordination polymer that is, $\{[Co_4(3\text{-dpyb})_2(odpa)_2(H_2O)_3]\cdot 4H_2O\}_n$ (**1**) [where 3-dpyb is *N*,*N*′-bis(3-pyridinecarboxamide)-1,4-butane, and H_4odpa represents 4,4′-oxydiphthalic acid] is produced through reaction between two organic ligands and $Co(NO_3)_2\cdot 6H_2O$ in the water and DMF mixed solvents. For the treatment of chronic nephritis, real time RT-PCR is employed for measuring the AMPK signaling pathway activation, and ELISA detection kit is applied to evaluate inflammatory cytokines content released into plasma. Computer simulation has revealed that the activity of the proposed candidate is only from the carboxyl function groups, however, nitrogen atoms from both amide and pyridine groups only showed limited activity to the protein.

Keywords: Coordination polymer, Chronic nephritis, Computer simulation

The design of coordination polymers (CPs) has attracted great attention because of their underlying extensive applications as the functional materials. Their architectures and performances come from a variety of molecular building blocks linked via supramolecular contacts and coordination bonds[1-4]. A large number of CPs have been recorded, like 1D ladders and chains, 2D meshes, 3D spiral staircase nets, interpenetrating patterns and microporous nets. Recently, special attention has been paid to the systems involving single pattern entanglements[5-8]. Nonetheless, the proper design and establishment of the required compounds is still a huge challenge. The architectures of metal organic frameworks (MOFs) established via supramolecular contacts and/or coordination bonds can be significantly changed through very small regulatory factors. Lots of factors, like solvent systems, organic ligands, counter ions and metal ions, have a great impact on the architectures, so it is hard for predicting the establishment of molecular structures[9-12]. Among them, the selection of ligands is a crucial factor. Relative positions, functional groups and donor atoms can directly change the skeleton architectures[13-16]. In addition, flexible ligands have received great interest on account of their flexible conformations, those are expected to generate many fascinating structures, for instance entanglement and polymorph, etc. A great deal of mixed-ligand MOFs are reported, exhibiting the combination of distinct ligands, which can produce greater architectural skeleton adjustability than the single ligands[17,18]. Therefore, mixed ligands are an excellent selection for constructing novel polymer structures. In this present research, through utilizing a mixed-ligand strategy, a Co(II) CP, that is, $\{[Co_4(3\text{-dpyb})_2(odpa)_2(H_2O)_3]\cdot 4H_2O\}_n$ (**1**) [where 3-dpyb is *N*,*N*′-bis(3-pyridinecarboxamide)-1,4-butane, and H_4odpa represents 4,4′-oxydiphthalic acid] was produced through reaction between two organic ligands and $Co(NO_3)_2\cdot 6H_2O$ in the water and DMF mixed solvents. Its application values on the chronic nephritis were evaluated and the detail mechanism simultaneously was investigated. The real time RT-PCR outcomes exhibited that this compound could remarkably down-regulated the AMPK signaling pathway activation levels. In addition, the ELISA analysis data reflected that the inflammatory cytokines content released into plasma was also suppressed through the as-produced compound. In order to provide further evidence above the experimental analysis, molecular docking simulation was performed.

Experimental Details

Chemicals and measurements

In this paper, the materials used were purchased from commercial sources and they utilized directly unless otherwise noted. With the aim of conducting

elemental analysis, Perkin-Elmer 2400C was employed. The FT-IR spectrometer of EQUINOX-55 was employed to record the IR spectra between 400 and 4000 cm^{-1}.

Preparation and characterization of $\{[Co_4(3\text{-dpyb})_2(odpa)_2(H_2O)_3]\cdot 4H_2O\}_n$ (1)

A mixture of $Co(NO_3)_2\cdot 6H_2O$ (0.060 g, 0.2 mmol), 3-dpyb (0.1 mmol, 0.030 g), and H_4odpa (0.035 g, 0.1 mmol) was stored in a stainless steel vessel (23 mL) lining by Teflon involving a mixed solvent of 2 mL DMA and 9 mL H_2O. It was subsequently heated for 96 h to 120 ℃ temperature. After cooling this mixture to room temperature, pink and transparent cubic crystals were generated, which were then air-dried for half a day (with 73% yield according to Co). Anal. calcd (%) for the $C_{32}H_{30}N_4Co_2O_{15}$: N, 6.76; C, 46.39 and H, 3.65. Found (%): N, 6.91; C, 46.53 and H, 4.02. IR (KBr, cm^{-1}): 3403 w, 3114 w, 2931 w, 1552s, 1506 w, 1403m, 1342 w, 1289m, 1147m, 1000 w, 771 w, 670 w.

The Oxford Xcalibur E diffractometer containing enhance (Mo) X-ray source was employed for collecting the X-ray data. CrysAlisPro was applied for the exploration of the strength data, which was subsequently converted to the HKL files. OLEX2 software with olex2.solve program together with the least-squares method based SHELXL (version: 2018/3) were respectively, employed to produce and modify the original architectural modes. The anisotropic parameters were mixed after using the whole non-H atoms. Eventually, the entire H-atoms could be fixed on the C atoms that they are linked to in geometry with AFIX commands. Crystal Data for **1** ($C_{64}H_{62}Co_4N_8O_{29}$, M =1642.93 g/mol): triclinic P-1 space group (no. 2), a = 11.2231(2) Å, b is equal to 12.9465(3) Å, c = 13.52360(10) Å, α = 61.6280(10)°, β = 68.967(2)°, γ = 76.025(2)°, V = 1607.72(6) $Å^3$, Z = 1, T = 273.15 K, μ(MoKα) = 1.114 mm^{-1}, $Dcalc$ = 1.697 g/cm^3, 12678 determined reflections (3.572° ≤ 2Θ ≤ 57.998°), 8433 unique (R_{sigma} is 0.0456 and R_{int} is 0.0194) which could be employed for all the calculations. The ultimate R_1 and wR_2 was 0.0471 (I > 2σ(I)) and 0.1322 (for all the data). CCDC number: 2047404.

AMPK signaling pathway activation

For the evaluation of the bio-activity of the compound, the *sirt1* and *ampk* genes relative expression levels after the exposure of compound was detected with real time RT-PCR. This investigation was completed strictly based on the instructions along with a little change. Shortly, fifty BALB/C mice (between 6 and 8 weeks, from 18 to 22g) were provided through the Experimental Animal Research Center of Nanjing University (Nanjing, China) and which were placed under 45 percent humidity at a temperature from 20 to 25 ℃ with free water and free food. The animal model of chronic nephritis was then created through injecting aminonucleoside, the treatment was subsequently conducted with compound at 1, 2 and 5 mg/kg concentration. After finishing the above treatment, the renal endothelial cells were gathered, and TRIzol reagent was employed for extracting total RNA in cells, which was transcripted reversely into the cDNA with kit based on the proposal of manufacturer after testing concentration. The *sirt1* and *ampk* relative expression was determined with SYBR Green Master Mix (Roche), where *gapdh* was applied as an internal control. The outcomes could be counted through $2^{-\Delta\Delta Ct}$ approach from three times conduction.

IL-6 and IL-18 measurement

The analysis of ELISA was implemented for assessing the IL-18 and IL-6 content released into plasma after compound treatment. This study was accomplished completely following the instructions of manufactures. Briefly, the animal model of chronic nephritis was then created through injecting aminonucleoside, the treatment was subsequently implemented after adding compound at 1, 2 and 5 mg / kg concentration. Then, the plasma in various animal was gathered and the IL-18 and IL-6 content released into plasma was detected for 3 or more times, and the acquired data were decreased with mean±SD.

Simulation details

To implement the simulation of molecular docking and to investigate the regulating energy metabolism, the repeat protein structure from AMP-activated protein kinase (AMPK) was chosen as the target protein, the protein data bank code was 4YEE[19]. The ligands from the proposed metal compound, as mentioned in the experimental section, were constructed by molecular generator Avogadro 1.2. It has to be mentioned here that only the representative short fragments from the metal compound are considered as effective ligand, since it has been shown that the metal compound would dissolve in the tested environment into short moieties, and therefore, we assume that the fragment is responsible for the real ligand-receptor interactions. Simple energy

optimizations were performed. Next, to build the initial binding conformations for both ligands, the AutoDockTools 1.5.6 was employed, explicitly, the grid box length could be set to 80, which was large enough for covering all the active sites which are placed on the surface of the target protein. The central coordinates of the grid box were 46.6, -14.4 and 8.4. The ligands were set to semiflexible and the target protein was set to rigid with the consideration of computational resources. Finally, AutoDock 4.2 was exploited to conduct simulation[20].

Results and Discussion

Crystal structure

The single crystal X-ray diffraction study exhibits that the compound **1** was crystallized in a triclinic space group of *P-1*. Fig. 1a illustrates that the fundamental unit of this compound is constructed from 2 Co(II) ions, a 3-dpyb, and a totally deprotonated ligand of odpa^{4-}. There exist two types of crystal nonequivalent cobalt ions having various coordinated manners: (i) Co1 ions combine with three O atoms provided by a disparate ligand of odpa^{4-} and a coordinated H_2O molecule, creating a twisted tetrahedral structure. (ii) The Co2 is 6-coordinated through two nitrogen atoms belong to two ligands of 3-dpyb, three oxygen atoms offered by three distinct ligands of odpa^{4-}, and 0.5 coordinated H_2O molecule, which reflects a twisted coordination structure of octahedron. The separation of Co–O bond is between 1.956(17) Å and 2.286(4) Å, this is similar to the lengths in formerly reported compounds[21-23]. As displayed in the Fig. 1b, 4 Co^{2+} ions are linked through 4 carboxyl groups derived from a ligand odpa^{4-} forming annular secondary building units $\{Co_4(COO)_4\}$. The above SBUs of $\{Co_4(COO)_4\}$ are bridged through odpa^{4-} producing a 2-dimensional Co_4-carboxylic layered architecture along plane *ac*. Besides, each SBU of $\{Co_4(COO)_4\}$ links four ligands of 3-dpyb originated from four various directions. It is worth nothing that the 3-dpyb are the classic flexible N-ligands, which exhibits two distinct distances of linked manners, denoted as 3-dpyb-b and 3-dpyb-a. For 3-dpyb-a, the length between the two nitrogen atoms of the two-terminal pyridine groups is 12.9 Å; It links the neighbouring Co2 atoms in Co_4 carboxyl 2-dimensional layer along plane *ac* (Fig. 1c), while

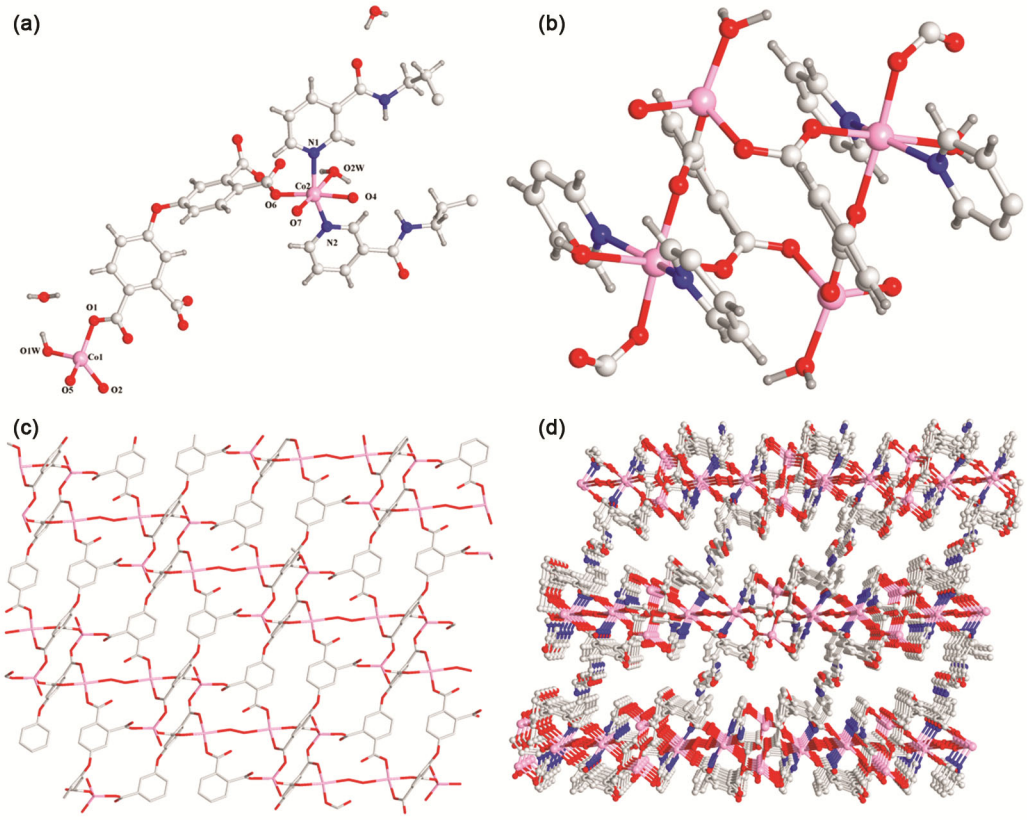

Fig. 1 — (a) The fundamental unit, (b) Co4 cluster, (c) 2-dimensional layered net and (d) 3-dimensional pillar layered network of compound **1**

3-dpyb-b is 14.3 Å, which is longer than 3-dpyb-a, linking the consecutive 2-dimensional layers into a 3-dimensional skeleton along plane *bc* (Fig. 1d).

To check the phase purity of the products, powder X ray diffraction (PXRD) experiments have been carried out for the as-prepared compound **1** (Fig. 2a).The peak positions of the experimental and simulated PXRD patterns are in good agreement with each other, indicating that the crystal structure is truly representative of the bulk crystal products. The differences in intensity may be owing to the preferred orientation of the crystal samples. Considering the following bioactivity tests, it is necessary to study the framework stability of compound **1** in the dispersing solvent DMSO and the simulated *in vivo* condition phosphate buffered saline (PBS). Due to compound **1** could not be dissolved in the organic solvents and water, we used its stock solution in the following bioactivity tests. With this in mind, about 100 mg of the as-prepared crystaline samples of **1** was taken in a mortar. It was then being ground manually for 30 min by using a pestle. The produced fine powders were soaked in 20 mL PBS or DMSO and subjected to the ultrasonic treatments for 2 h to obtain the well dispersed solution. After keeping for two days, the fine powder was recovered via centrifugation and their PXRD measurements show that the PXRD profiles of the treated samples show good matches with those of the as-prepared samples, reflecting their good stability in the above conditions (Fig. 2). In the IR spectra of **1**, the absorption band at 3403 cm^{-1} can be assigned to the stretching vibration of hydroxyl (O–H) group, suggesting the presence of water molecules in **1**. The weak bands at 3114 cm^{-1} can be assigned to ν(Ar–H) of ligands. The bands of **1** at 2931 cm^{-1} can be attributed to the ν(C–H) of methyl group in 3-dpyb ligands. The characteristic bands of carboxyl groups in **1** are shown at 1552 and 1403 cm^{-1}. The respective values of ($\nu_{asym}(COO^-)$-$\nu_{sym}(COO^-)$) (149 cm^{-1} for **1**) suggest the presence of chelating coordination mode of the carboxylate groups in $odpa^{4-}$ ligand. The absence of the expected absorption bands at around 1700 cm^{-1} for the protonated carboxyl group indicates that all carboxyl groups of H_4odpa have been deprotonated. The bands at 1342 and 1289 cm^{-1} as well as those from 1000 to 670 cm^{-1} in **1**, should be attributed to the pyridine of the 3-dpyb ligands. These spectral informations are consistent with the results of the single-crystal X-ray diffraction analyses.

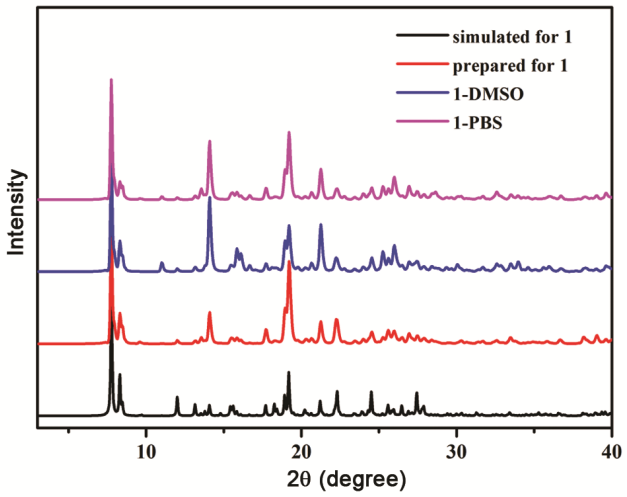

Fig. 2 — The PXPRD patterns for compound 1

Inhibition of AMPK signaling pathway activation

After forming the above mentioned compound, the inhibitory activity of this compound on the signaling pathway of AMPK was assessed through real time RT-PCR via the determination of the *sirt1* and *ampk* genes relative expression. The information in Fig. 3 exhibited that model group has an evidently up-regulated *sirt1* and *ampk* genes level in comparison with control group. Nonetheless, after treating through the above compound, the *sirt1* and *ampk* genes relative expression levels were markedly decreased. The suppression of expression of genes revealed a dose dependent correlation.

Reduction of inflammatory cytokines content in plasma

In the above experiment, we have confirmed that the compound could markedly down-regulate the AMPK signaling pathway activation, described as the down-regulated *sirt1* and *ampk* genes expression levels. Moreover, the IL-18 and IL-6 inflammatory cytokines content released into plasma was tested through specific ELISA assay kit. As the data

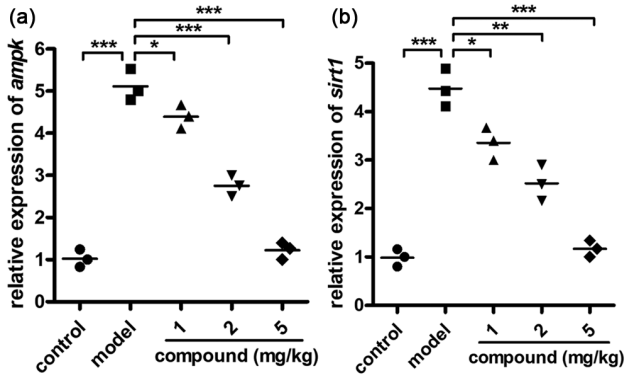

Fig. 3 — Plots relative expression for (a) *ampk* and (b) *sirt1* genes versus different concentration of the compound **1** used

exhibited in Fig. 4, it can be observed that model group possesses much higher IL-18 and IL-6 content than control group. After the compound exposure, the IL-18 content and IL-6 content released into plasma was suppressed evidently.

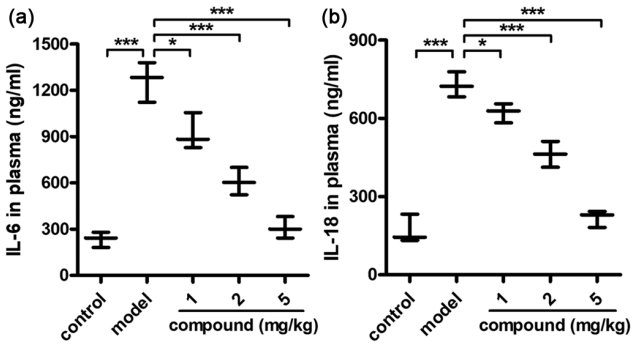

Fig. 4 — Plots between the (a) IL-18 content and (b) IL-6 content released into plasma was then examined through applying ELISA assay kit by using different concentration of the compound **1** used

Molecular docking

The beta2 carbohydrate binding module on the AMPK protein has been reported that it may have greater affinity for partially degraded glycogen, and it is important in regulating energy metabolism in all eukaryotes[19], which makes it a very suitable target protein for investigating the activity for chronic nephritis diseases. As mentioned in experimental section, the proposed metal compound has two ligands, one ligand is a carboxyl group rich structure, and the second contains potential nitrogen atoms from both amide and pyridine groups. Thus their interactions with the target protein were estimated by computer simulation for understanding the activities that were found in experiment.

The binding conformations between the ligands and the target protein were shown in Fig. 5. It can be seen in Fig. 5a that the carboxyl group rich ligands showed multiple binding interactions, the calculated

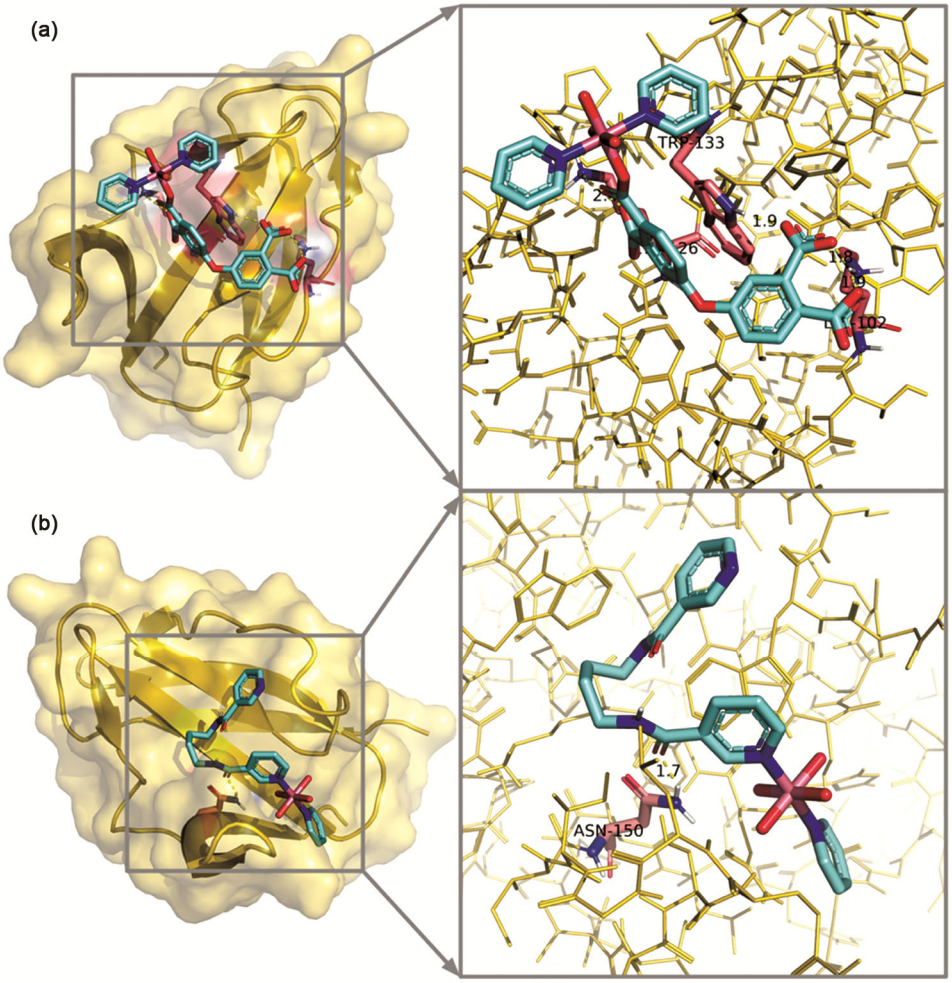

Fig. 5 — Binding conformations for (a) carboxyl rich ligand and (b) flexible ligand which contains amide and pyridine groups. The binding interactions as well as their corresponding lengths are shown in detail

affinity energy was -8.7 kcal/mol. From the inset of Fig. 5a four binding interactions were found, the involving residues that provided active sites were LYS-102 (1.8 and 1.9 Å), TRP-133 (1.9 Å) and LYS-126 (2.4 Å), for all the observed binding interactions, the carboxyl group provided the oxygen atom as the donor for the hydrogen bond. In comparison, from Fig, 5b it can be seen that only one binding interaction was formed, the oxygen from amide group was interacting with residue ASN-150 with the binding distance of 1.7 Å, furthermore, we can see that the -NH group on the ligand was actually the accepter of the hydrogen bond, where the -C=O group on the residue ASN-150 was the donor. The calculated affinity energy was about -5.8 kcal/mol. The above results pointed out that both ligands were showing possible activities toward the target protein, from number of binding interactions and the affinity energies it can be concluded that the carboxyl group rich ligand was the main source of biological activity.

Conclusion

On the whole, we have synthesized a Co(II) coordination polymer in success with a reaction between two organic ligands and $Co(NO_3)_2 \cdot 6H_2O$ in water and DMF mixed solvents. The as-prepared coordination polymer **1** has been studied via EA and the diffraction of single crystal X-ray. The analysis for the single crystal X-ray diffraction suggests that the **1** has a 3-dimensional pillar-layered framework based on the Co_4-carboxylic 2D layer and the 3-dpyb pillar. The real time RT-PCR outcomes revealed that this compound could evidently down-regulate the AMPK signaling pathway activation levels. Moreover, the analysis of ELISA suggested that the inflammatory cytokines content released into plasma was also suppressed through our novel compound. Based on the findings from molecular docking results it can be concluded that the activity of the proposed candidate was mainly from the carboxyl functional groups, however, nitrogen atoms from both amide and pyridine groups only showed limited activity to the protein. Eventually, we can acquire the information that this compound possessed superb treatment activity against the chronic nephritis through suppressing the AMPK signaling pathway activation and inflammatory response.

Reference

1 Feng X, Feng Y Q, Chen J J, Ng S W, Wang L Y & Guo J Z, *Dalton Trans,* 44 (2015) 804.

2 Bharati A K, Somnath, Lama P & Siddiqui K A, *Inorg Chim Acta,* 500 (2020) Article 119219.

3 Raja D S, Ramachandran E, Bhuvanesh N S P & Natarajan K, *Eur J Med Chem,* 64 (2013) 148.

4 Fan L, Zhao D, Zhang H, Wang F, Li B, Yang L, Deng Y & Zhang X, *Micropor Mesopor Mat*, 326 (2021) 111396.

5 Zhao D, Song J, Zhang X, Wang F, Li B, Yang L, Deng Y, Li Q & Fan L, *CrystEngComm*, 23 (2021) 6245.

6 Shigematsu A, Yamada T & Kitagawa H, *J Am Chem Soc,* 134 (2012) 13145.

7 Liu J J, Xia S B, Duan Y L, Liu T, Cheng F X & Sun C K, *Polymers (Basel),* 10 (2018) 165.

8 Li B, Zhao D, Wang F, Zhang X, Li W & Fan L, *Dalton Trans*, 50 (2021) 14967.

9 Li R F, Li R H, Liu X F, Chang X H & Feng X, *RSC Adv*, 10 (2020) 6192.

10 Han Z, Yu Y, Zhang Y, Dong B, Kong A & Shan Y, *J Mater Chem A,* 3 (2015) 23716.

11 Li R F, Zhang Y W, Liu X F, Chang X H & Feng X, *Inorg Chim Acta*, 502 (2020) 119370.

12 Gu J Z, Liang X X, Cui Y H, Wu J, Shi Z F & AM Kirillov, *CrystEngComm,* 19 (2017) 2570.

13 Zhang X, Hou L, Liu B, Cui L, Wang Y Y & Wu B, *Cryst Growth Des,* 13 (2013) 3177.

14 Shigematsu A, Yamada T & Kitagawa H, *J Am Chem Soc,* 134 (2012) 13145.

15 Zhu J, Li P Z, Guo W, Zhao Y & Zou R, *Coord Chem Rev*, 359 (2018) 80.

16 Cui J W, Hou S X, Van Hecke K & Cui G H, *Dalt Trans,* 46 (2017) 2892.

17 Gao P F, Zheng L L, Liang L J, Yang X X, Li Y F & Huang C Z, *J Mater Chem B,* 1 (2013) 3202.

18 Seco J M, Oyarzabal I, Pérez-Yáñez S, Cepeda J & Rodríguez-Diéguez A, *Inorg Chem,* 55 (2016) 11230.

19 Mobbs J I, Koay A, Paolo A D, Bieri M, Petrie E J, Gorman M A, Doughty L, Parker M W, Stapleton D I, Griffin M D W & Gooley P R, *Biochem J,* 468 (2015) 245.

20 Morris G M, Huey R, Lindstrom W, Sanner M F, Belew R K, Goodsell D S & Olson A J, *J Comput Chem,* 16 (2009) 2785.

21 Gu J, Wen M, Cai Y, Shi Z, Nesterov D S, Kirillova M V & Kirillov A M, *Inorg Chem,* 58 (2019) 5875.

22 Xiao Q Q, Dong G Y, Li Y H & Cui G H, *Inorg Chem,* 58 (2019) 15696.

23 Arici M, Yeşilel O Z, Taş M & Demiral H, *Cryst Growth Des,*17 (2017) 2654.